

# Testing the Scale Dependence of the Scale Factor $\sigma_{\text{eff}}$ in Double Dijet Production at the LHC

Svend Domdey<sup>1,2\*</sup>, Hans-Jürgen Pirner<sup>†1</sup> and Urs Achim Wiedemann<sup>‡2</sup>

<sup>1</sup>*Institut für Theoretische Physik, Philosophenweg 19, D-69120 Heidelberg, Germany*

<sup>2</sup>*Department of Physics, CERN, Theory Division, CH-1211 Genève 23, Switzerland*

The scale factor  $\sigma_{\text{eff}}$  is the effective cross section used to characterize the measured rate of inclusive double dijet production in high energy hadron collisions. It is sensitive to the two-parton distributions in the hadronic projectile. In principle, the scale factor depends on the center of mass energy and on the minimal transverse energy  $E_{\text{T,min}}$  of the jets contributing to the double dijet cross section. Here, we point out that proton-proton collisions at the LHC will provide for the first time experimental access to these scale dependences in a logarithmically wide, nominally perturbative kinematic range  $10 \text{ GeV} \lesssim E_{\text{T,min}} \lesssim 100 \text{ GeV}$ . This constrains the dependence of two-parton distribution functions on parton momentum fractions and parton localization in impact parameter space. Novel information is to be expected about the transverse growth of hadronic distribution functions in the range of semi-hard Bjorken  $x$  ( $0.001 \lesssim x \lesssim 0.1$ ) and high resolution  $Q^2$ . We discuss to what extent one can disentangle different pictures of the  $x$ -evolution of two-parton distributions in the transverse plane by measuring double-hard scattering events at the LHC.

## I. INTRODUCTION

In high-energy hadronic collisions, more than one pair of partons can interact with large momentum transfer. Such multiple hard interactions within the same hadronic collision become more numerous with increasing center of mass energy. They are a novel and generic feature of hadronic interactions at Tevatron and at the LHC. For instance, the inclusive cross section for double dijet production (see Fig. 1) is  $\sigma_D(E_{\text{T,min}} = 20 \text{ GeV}) \simeq 10 \mu\text{b}$  in proton-proton

---

\* Email: domdey@tphys.uni-heidelberg.de

† Email: pir@tphys.uni-heidelberg.de

‡ Email: Urs.Wiedemann@cern.ch

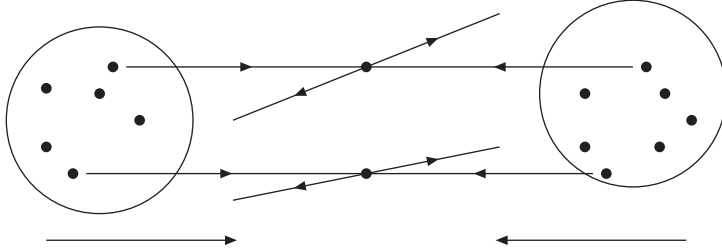


FIG. 1: Schematic view of double dijet production in a proton-proton collision.

collisions at the LHC, if each of the four jets carries more than a minimal transverse energy of  $E_{T,\min} = 20$  GeV. Even if this threshold is raised to  $E_{T,\min} = 100$  GeV, the double hard scattering process is still in experimental reach with  $\sigma_D^{4\text{jets}}(E_{T,\min} = 100 \text{ GeV}) \simeq 50 \text{ pb}$ . We will present calculations, supporting these estimates, in section II.

It is not known how factorization theorems for large momentum transfer processes could be extended to multiple hard processes within the same hadronic collision, such as double dijet production. Typically, one assumes that such processes can be described as the incoherent superposition of single hard scattering processes [1, 2, 3, 4, 5]. The double dijet cross section can then be expressed as the convolution of two independent hard partonic subprocesses with two-parton distribution functions  $F_D$  (see eq. (2.3) below). The ratio of the square of the dijet cross section  $\sigma_S$  to the double dijet cross section  $\sigma_D$  for two indistinguishable hard processes defines the effective cross section  $\sigma_{\text{eff}}$  [2, 6, 7]

$$\sigma_{\text{eff}} = \frac{\sigma_S^2}{2\sigma_D}. \quad (1.1)$$

For two distinguishable hard processes  $A$  and  $B$ , it takes the form  $\sigma_{\text{eff}} = \frac{\sigma_A \sigma_B}{\sigma_D}$ . If the two-parton distribution functions  $F_D$  factorize into an uncorrelated product of standard single parton distribution functions, then  $\sigma_{\text{eff}}$  gives access to the geometrical extension of the parton distributions in transverse space.

There are several motivations for studying double hard cross sections at hadron colliders. First, hadronic collisions with more than one hard partonic scattering can contribute to multi-parton final states at high transverse momentum. Their improved understanding may help to control the QCD background to searches for novel physics in channels involving multiple high- $E_T$  parton final states [8], although simple kinematic cuts can be efficient in cleaning the signal from double dijet background [5]. Second, multiple independent hard scatterings at

lower momentum transfers [ $Q^2 \sim O((1-5)^2 \text{ GeV}^2)$ ] play an important role in modeling the underlying event in hadronic collisions at collider energies [9, 10, 11]. Studying the physics of such multiple hard scatterings at larger momentum transfer  $Q^2$  or as a function of  $Q^2$  may help to constrain the input to this modeling of the underlying event [12]. Moreover, the double dijet cross section  $\sigma_D$  provides qualitatively novel information about the transverse structure of the hadronic projectile because  $\sigma_D$  depends on the relative transverse distribution of the two partons in the hadronic projectile [13]. If the two partons were distributed homogeneously over the entire hadronically active transverse area of the hadronic projectile, then the scale factor  $\sigma_{\text{eff}}$  would be comparable to the total inelastic cross section. The much smaller numerical value  $\sigma_{\text{eff}} = 14.5 \pm 1.7_{-2.3}^{+1.7}$  mb, measured by the CDF Collaboration [7] disfavors such a homogeneous distribution. It is in support of a picture of the proton and anti-proton, in which partons with large momentum fraction are localized in a significantly smaller transverse region within the proton (see discussion of Fig. 2 below).

Quantum chromodynamics offers a specific picture for the transverse growth of hadronic wave functions with increasing  $\ln 1/x$  or center of mass energy. In analogy to QED, where the transverse extension of the Weizsäcker-Williams field of quasi-real photons around an electric charge grows with increasing energy, the hard (i.e. large- $x$ ) color charges in a QCD projectile can be viewed as sources of non-abelian Weizsäcker-Williams fields, whose transverse size grows with increasing  $\ln 1/x$  or center of mass energy. The simplest, perturbative realization of this phenomenon in QCD is the BFKL evolution equation, which predicts with increasing  $\ln 1/x$  not only a growth of parton density locally in impact parameter, but also a growth of the hadronic projectile distribution function in impact parameter space, see e.g. Refs. [14, 15, 16, 17, 18]. Unlike QED, this perturbative picture is expected to be modified in QCD by saturation effects, which tame the growth of parton density locally in impact parameter, and by non-perturbative effects, which amputate the gluonic Weizsäcker-Williams fields at a transverse distance set by confinement. One expects that this reduces eventually the growth of the average transverse extension of non-abelian Weizsäcker-Williams fields from the perturbatively predicted power-law dependence  $\propto x^{-\omega}$  to a non-perturbative logarithmic increase. The scale and dynamics of the transition between perturbative and non-perturbative regime, as well as the physics in the non-perturbative regime remain under debate. All arguments indicate, however, that the transverse extension of the hadronic densities continues to grow at ultra-relativistic center of mass energies, albeit possibly much weaker than predicted perturbatively [14, 17, 18].

Here, we investigate to what extent this qualitative picture of the growth of transverse hadronic distributions could be tested by measuring double dijet production at Tevatron and at the LHC in the range of semi-hard momentum fractions, say  $0.001 \lesssim x \lesssim 0.1$ , and hard momentum transfers. The starting point of our work is the observation that measurements of the inclusive double dijet cross section at the LHC can be performed over a wide range in  $E_{T,\min}$ . In the following, we quantify this range and we investigate to what extent it provides access to a possible dependence of the scale factor on the cm-energy and transverse momentum cut-off. On the basis of these calculations, we assess the sensitivity of measurements of  $\sigma_D$  to the transverse growth of the distribution of semi-hard partons in the hadronic projectile.

## II. THE FORMALISM

We first discuss the formalism, on which the following calculations of double dijet production cross sections are based. To leading order (LO), the single scattering cross section to produce two massless partons of transverse energy larger than  $E_{T,\min}$  reads

$$\sigma_S(E_{T,\min}) = \int_{x_{\min}}^1 dx_1 \int_{x_{\min}/x_1}^1 dx_2 \int_{\hat{t}_-}^{\hat{t}_+} d\hat{t} \sum_{ij} f_i(x_1, Q^2) f_j(x_2, Q^2) \frac{d\sigma^{ij}}{d\hat{t}}, \quad (2.1)$$

where

$$\hat{t}_{\pm} = -\frac{\hat{s}}{2} \left( 1 \pm \sqrt{1 - \frac{4 E_{T,\min}^2}{\hat{s}}} \right), \quad x_1 x_2 \geq x_{\min} = \frac{4 E_{T,\min}^2}{s} \quad \text{and} \quad Q^2 = p_{\perp}^2. \quad (2.2)$$

The sum is over all possible quark and gluon  $2 \rightarrow 2$  scattering channels  $ij$ . For the purpose of the present study, expression (2.1) is a sufficiently good approximation for the cross section of a dijet, produced in a single hard scattering event. We shall convolute LO parton-parton scattering cross sections  $\frac{d\sigma^{ij}}{d\hat{t}}$  with the CTEQ6L set of parton distribution functions [19] for  $f_i$ , which have been optimized for the use in LO calculations. The scale  $Q^2$  in the PDFs and in  $\alpha_s$  is set to the transverse momentum  $p_{\perp}^2 = ut/s$  for massless partons in the  $2 \rightarrow 2$  process. We have checked that the results for  $\sigma_S(E_{T,\min})$  obtained with this input from Eq.(2.1) are consistent with Pythia 6.419 [20].

We calculate the inclusive dijet production cross section as an incoherent superposition of two hard scattering processes within the same hadronic collision

$$\sigma_D(E_{T,\min}) = \frac{1}{2} \sum_{ijkl} \int ds_1 ds_2 d\mathbf{b} \int dx_1 dx_2 dx_3 dx_4 d\hat{t}_1 d\hat{t}_2 F_D^{ik}(x_1, x_2; \mathbf{b} - \mathbf{s}_1, \mathbf{b} - \mathbf{s}_2)$$

$$\times F_D^{jl}(x_3, x_4; \mathbf{s}_1, \mathbf{s}_2) \frac{d\sigma^{ij}}{d\hat{t}_1} \frac{d\sigma^{kl}}{d\hat{t}_2}. \quad (2.3)$$

Here, the sum  $\sum_{ijkl}$  is over all parton species, which contribute to the two partonic processes  $i+j \rightarrow 2$  jets and  $k+l \rightarrow 2$  jets. The symmetry factor  $\frac{1}{2}$  accounts for the fact that both partonic processes are indistinguishable in the sense that there is no operational prescription which establishes a one-to-one mapping between one dijet and one specific hard partonic cross section in (2.3). The Mandelstam variables  $\hat{t}_1$  and  $\hat{t}_2$  are defined for two partonic  $2 \rightarrow 2$  processes with incoming parton momentum fractions  $x_1, x_3$  and  $x_2, x_4$ , respectively. We choose the kinematic boundaries in the integrals over the incoming parton momentum fractions  $x_1, \dots, x_4$  such that all outgoing partons carry more than a minimal transverse energy  $E_{T,\min}$ . (In principle, more sophisticated kinematic boundaries could be implemented e.g. to require different  $E_{T,\min}$ -values for both pairs of jets, but we shall not explore such possibilities in the following.) The integral in equation (2.3) includes the two transverse positions  $\mathbf{s}_1, \mathbf{s}_2$ , at which the two hard processes take place, and the impact parameter  $\mathbf{b}$  of the hadronic collision. The spatial information about the partons is specified in the two-parton distribution functions

$$F_D^{ik}(x_1, x_2; \mathbf{b}_1, \mathbf{b}_2; Q_1^2, Q_2^2), \quad (2.4)$$

which depend not only on the transverse momentum fractions  $x_1, x_2$  and the virtualities  $Q_1^2, Q_2^2$  of both partons inside the hadron, but also on their transverse positions  $\mathbf{b}_1, \mathbf{b}_2$ . In the following, we shall often use a simplified notation, in which the virtualities are not written explicitly as arguments of  $F_D$ . For these virtualities, we will always choose the squared transverse momenta in the corresponding partonic  $2 \rightarrow 2$  subprocess, as in (2.1), (2.2).

### A. A factorized ansatz for two-parton distribution functions

The discussion in this section is based on a class of models, which satisfy the factorized ansatz

$$F_D^{ik}(x_1, x_2; \mathbf{b}_1, \mathbf{b}_2; Q_1^2, Q_2^2) = F^i(x_1, \mathbf{b}_1, Q_1^2) F^k(x_2, \mathbf{b}_2, Q_2^2), \quad (2.5)$$

where

$$F^i(x, \mathbf{b}, Q^2) = n(x, \mathbf{b}) f^i(x, Q^2). \quad (2.6)$$

A set of correlated two-parton distributions, which do not satisfy (2.5) will be discussed in section IV. In equation (2.6),  $n(x, \mathbf{b})$  denotes the density of partons in the transverse plane.

It is normalized to unity,  $\int d\mathbf{b} n(x, \mathbf{b}) = 1$ , so that  $f^i(x, Q^2) = \int d\mathbf{b} F^i(x, \mathbf{b}, Q^2)$  are the standard single parton distribution functions. For the class of models studied here, the transverse part of the density does not depend on the parton species  $i$ . The ansatz of Eq. (2.6) contains information about the average transverse distance of the partons from the center of the proton in transverse space. If the partons are uncorrelated in impact parameter, the average distance between the two partons satisfies  $\langle (\mathbf{b}_1 - \mathbf{b}_2)^2 \rangle = \langle \mathbf{b}_1^2 \rangle + \langle \mathbf{b}_2^2 \rangle$ . In this sense, the ansatz (2.5) also contains information about the average transverse distance between the two partons. In addition, it allows for a non-trivial  $x$ -dependence of the transverse size of the hadronic projectiles.

Let us consider first the simple case of an  $x$ -independent density  $n(x, \mathbf{b}) = n(\mathbf{b})$ . In this case, the geometrical information entering cross sections can be expressed in terms of the nucleon overlap function

$$T_{\text{NN}}(\mathbf{b}) = \int d\mathbf{s} n(\mathbf{s}) n(\mathbf{b} - \mathbf{s}). \quad (2.7)$$

The normalization of  $n$  implies that  $\int d\mathbf{b} T_{\text{NN}}(\mathbf{b}) = 1$ . For the factorized ansatz (2.5), the double dijet cross section then takes the form

$$\sigma_D(E_{\text{T,min}}) = [\sigma_S(E_{\text{T,min}})]^2 \frac{1}{2} \int d\mathbf{b} T_{\text{NN}}^2(\mathbf{b}), \quad (2.8)$$

and the scale factor (1.1) reads

$$\sigma_{\text{eff}} = \frac{1}{\int d\mathbf{b} T_{\text{NN}}^2(\mathbf{b})}. \quad (2.9)$$

In the general  $x$ -dependent case, the nuclear overlap function (2.7) will depend on the momentum fractions  $x_1, \dots, x_4$  of the partons in both hadrons. As a consequence, the scale factor becomes a function of the center of mass energy  $\sqrt{s}$  and the jet energy threshold  $E_{\text{T,min}}$ .

## B. Interpretation of the scale factor in the model (2.5) for two-parton distributions

For the class of models (2.5), the scale factor contains information about the transverse parton density  $n(\mathbf{b})$  in the proton. A model-independent understanding of the  $\mathbf{b}$ -dependence of this density distribution is missing so far. Here, we consider three-dimensional density profiles, from which transverse densities are obtained by projection,  $n(\mathbf{b}) = \int dz n(\mathbf{r})$ . Rather than motivating a particular  $\mathbf{b}$ -dependence of  $n(\mathbf{b})$ , however, we prefer here to demonstrate that our conclusions about the scale factor will depend mainly on the rms of  $n(\mathbf{r})$  and will be

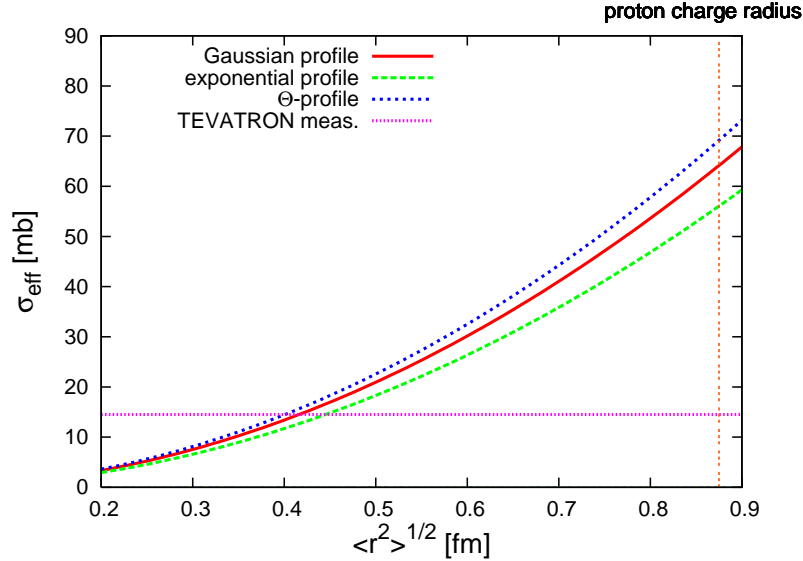


FIG. 2: The scale factor  $\sigma_{\text{eff}}$  as a function of the 3-dimensional rms of the parton density distribution for a Gaussian, exponential and  $\Theta$ -profile  $n(\mathbf{r})$ . The thinly dotted line denotes the central value of the Tevatron measurement  $\sigma_{\text{eff}} = 14.5$  mb. The value  $\langle r^2 \rangle^{1/2} = 0.875$  fm of the proton charge radius is also indicated.

rather insensitive to details of the functional shape. To establish this point, we compare three 3-dimensional parton densities  $n(\mathbf{r})$ . In particular, we consider a Gaussian density

$$n(\mathbf{r}) = \frac{1}{(2\pi\delta^2)^{3/2}} \exp\left[-\frac{\mathbf{r}^2}{2\delta^2}\right], \quad (2.10)$$

a homogeneous density distribution which is sharply cut at radius  $R$ ,

$$n(\mathbf{r}) = \frac{3}{4\pi R^3} \Theta(R - |\mathbf{r}|), \quad (2.11)$$

and an exponential profile

$$n(\mathbf{r}) = \frac{1}{8\pi\lambda^3} \exp\left[-\frac{|\mathbf{r}|}{\lambda}\right], \quad (2.12)$$

which has a more pronounced tail than the Gaussian distribution. To compare the sensitivity of  $\sigma_{\text{eff}}$  on the functional shape of the  $\mathbf{r}$ -dependence of the density profiles (2.10), (2.11) and (2.12), we express the results in Figure 2 and Table I in terms of the root mean square  $\langle r^2 \rangle^{1/2}$  of these densities.

One sees in Figure 2 that the numerical value of  $\sigma_{\text{eff}}$  characterizes mainly  $\langle r^2 \rangle^{1/2}$  and that its sensitivity to the detailed geometrical profile of  $n(\mathbf{r})$  is rather weak. As a consequence, the use of the Gaussian ansatz in the following studies can be regarded as a convenient choice which

Model for 3D density	ms radius $\langle \mathbf{r}^2 \rangle$	$\sigma_{\text{eff}}$	$\langle \mathbf{r}^2 \rangle_{\text{TEVATRON}}$
Gaussian $\propto \exp(-\frac{\mathbf{r}^2}{2\delta^2})$	$3\delta^2$	$\frac{8\pi}{3}\langle \mathbf{r}^2 \rangle$	0.42 fm
hard sphere $\propto \Theta(R -  \mathbf{r} )$	$\frac{3}{5}R^2$	$9.0 \langle \mathbf{r}^2 \rangle$	0.40 fm
exponential $\propto \exp(-\frac{ \mathbf{r} }{\lambda})$	$12\lambda^2$	$7.3 \langle \mathbf{r}^2 \rangle$	0.45 fm

TABLE I: Results from the spatial density analysis. Calculations of ms radius  $\langle \mathbf{r}^2 \rangle$  and  $\sigma_{\text{eff}}$  are shown for several density models. The last column is calculated by equating the  $\sigma_{\text{eff}}$  in the 4th column to the TEVATRON measurement of 14.5 mb. See also Fig. 2.

will not bias our conclusions. We mention as an aside that a Gaussian profile may be motivated for instance by a study based on a light cone Hamiltonian [21].

Figure 2 also demonstrates that the central value  $\sigma_{\text{eff}} = 14.5 \text{ mb}$  of the CDF measurement can be related to a narrow range around  $\langle \mathbf{r}^2 \rangle^{1/2} \simeq 0.4 - 0.45 \text{ fm}$  for all three geometrical profiles. We note that if the partons relevant for double dijet production were distributed in impact parameter over a transverse region of the size of the proton's electric charge  $\langle \mathbf{r}^2 \rangle^{1/2} = 0.875 \text{ fm}$ , then the scale factor  $\sigma_{\text{eff}}$  would take values between 50 mb and 70 mb, which are comparable to the total inelastic cross section  $\sigma_{\text{inel}} \simeq 80 \text{ mb}$  measured at Tevatron. A significant difference between the total hadronically active transverse size of the proton and the transverse extension of the region relevant for processes of high momentum transfer has been discussed repeatedly in the literature [18, 24, 27]. We note that the measurement of  $\sigma_{\text{eff}}$  can not only provide an independent characterization of this difference. Moreover, it may also provide novel access to the dynamical origin of this difference via an analysis of the  $x$ -dependence of  $\sigma_{\text{eff}}$ , to which we turn now.

### C. Modeling the small- $x$ evolution of the transverse size of hadronic wave functions

The transverse size of hard partonic components of the proton is found to be smaller than total cross sections but will also grow with increasing  $\sqrt{s}$ . Therefore a larger part of the hadronically active regions in transverse space can be expected to contribute to hard production processes with increasing energy.

We model this picture of the transverse growth of hadronic wave functions by specifying an  $x$ -dependence of the Gaussian density (2.11),

$$n(x, \mathbf{b}) = \frac{1}{2\pi\delta(x)^2} \exp\left[-\frac{\mathbf{b}^2}{2\delta(x)^2}\right]. \quad (2.13)$$

We consider two parametrizations of the  $x$ -dependence of the Gaussian width  $\delta(x)$ . One model, originally proposed by Burkardt [22], takes

$$\delta(x) = w_1 \sqrt{(1-x) \ln(1/x)}, \quad w_1 = 0.149 \text{ fm}. \quad (2.14)$$

This results in a growth of the scale factor  $\sigma_{\text{eff}}(x) \propto \delta^2(x) \propto \ln 1/x \propto \ln s$ , which is even weaker than the growth  $\propto (\ln s)^2$  which is realized in the Froissart bound. We fix the prefactor at  $w_1 = 0.149 \text{ fm}$  to reproduce the Tevatron value for  $\sigma_{\text{eff}}$  at  $E_{\text{T,min}} = 20 \text{ GeV}$ .

We also consider a second model which results in a power-law growth of  $\sigma_{\text{eff}} \propto s^\omega$  with the center of mass energy,

$$\delta(x) = w_2 (1-x) x^{-\omega/2}, \quad w_2 = 0.175 \text{ fm}. \quad (2.15)$$

A power-law growth of the transverse hadronic wave function is obtained in the perturbative small- $x$  evolution, where the leading order BFKL-intercept is  $\omega = \frac{\alpha_s}{\pi} N_c 4 \ln 2$ . This is known to overestimate the growth of total cross sections in the experimentally accessible regime. However, it is conceivable that the growth of hard components in the transverse wave function is more rapid. Within the window of physically reasonable parameters, we have chosen  $\omega = 0.265$  to arrive at a model with power-like growth at small  $x$ . The prefactor in (2.15) is fixed to  $w_2 = 0.175 \text{ fm}$  such that  $\sigma_{\text{eff}} = 14.5 \text{ mb}$  at  $\sqrt{s} = 1.8 \text{ TeV}$  and  $E_{\text{T,min}} = 20 \text{ GeV}$ .

In Fig. 3 we show the transverse growth of the width  $\langle \mathbf{b}^2 \rangle = 2\delta^2(x)$  as a function of momentum fraction  $x$  for the models (2.14) and (2.15). We note that a transverse growth similar to the model (2.14) has also been obtained in other calculations which model non-perturbative effects [18].

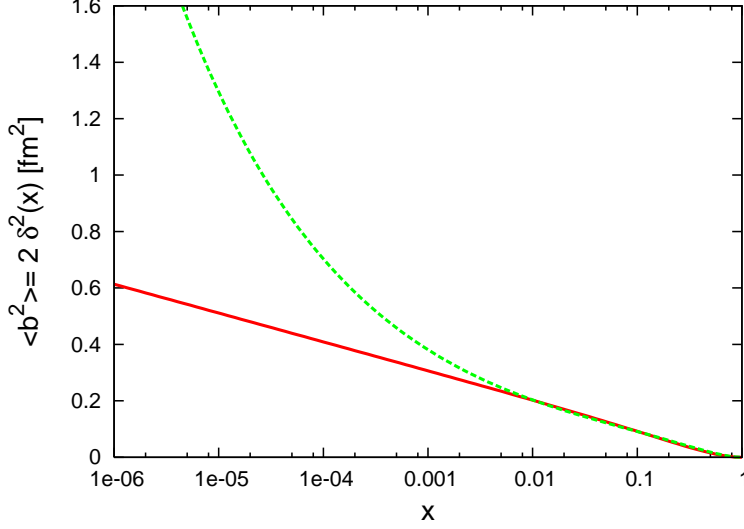


FIG. 3: Two models for the increase of  $\langle \mathbf{b}^2 \rangle = 2\delta^2(x)$  towards small  $x$  of the transverse proton wave function as a function of the parton momentum  $x$ . The lower (logarithmic) curve is a model (2.14) proposed by Burkardt [22], the upper (power-like) curve is discussed in eq. (2.15).

A comment about our use of CDF measurements is needed here: in the CDF publication [6] of 1993, a central value  $\sigma_{\text{eff}} = 12.1 \text{ mb}$  was quoted for  $E_{T,\text{min}} = 18 \text{ GeV}$  on the parton level. The later CDF measurement [7] quotes a central value  $\sigma_{\text{eff}} = 14.5 \text{ mb}$  with much improved statistical and systematic uncertainties. However, both CDF measurements considered a channel with three jets and one photon in the final state, while we focus on four jet processes in the present discussion. The possibility that the scale factor differs for different channels due to their dependences on different parton distribution functions, cannot be excluded and has been explored in a recent model study [23]. To arrive at a particularly simple model, and since there is little phenomenological guidance, we do not explore the possibility of such differences here. We also remark that the more recent CDF analysis uses several lower values of  $E_{T,\text{min}}$ . For these reasons, we emphasize that our choice  $\sigma_{\text{eff}}(\sqrt{s} = 1.8 \text{ TeV}, E_{T,\text{min}} = 20 \text{ GeV}) = 14.5 \text{ mb}$  does not reproduce the cuts and conditions of the CDF analysis. In particular, our choice of  $\sigma_{\text{eff}} = 14.5 \text{ mb}$  can only be related to the CDF analysis under the assumption that the scale factor does not depend on the production channel. Moreover, our choice of  $E_{T,\text{min}}$  is dictated by the need of anchoring our discussion at a sufficiently large transverse energy  $E_{T,\text{min}}$ , where the perturbative cross sections used in our calculations are sufficiently reliable.

### III. NUMERICAL RESULTS FOR $\sigma_{\text{eff}}$ FROM DOUBLE HARD CROSS SECTIONS

In this section, we first characterize the range of  $E_{T,\text{min}}$ , which is experimentally accessible with sufficiently large event samples for the study of double dijet production at Tevatron and at the LHC. We then discuss the scale dependence of  $\sigma_{\text{eff}}$  in the model (2.14) of Burkardt and in the BFKL model (2.15). Finally, we turn to the question to what extent more complicated geometrical arrangements of two-parton distributions, or correlations not encoded for in the ansatz (2.5) can affect our conclusions.

#### A. Rate of inclusive double 2-jet processes

Figure 4 shows the calculated cross section  $\sigma_S$  for inclusive 2-jet production and an estimate of the double dijet cross section  $\sigma_D$  as a function of the minimal transverse energy of the jets. To arrive at this estimate, the double dijet cross sections  $\sigma_D$  in Figure 4 is calculated from the single inclusive cross section  $\sigma_S$  using equation (1.1) with a scale-independent value  $\sigma_{\text{eff}} = 14.5 \text{ mb}$ . If  $\sigma_{\text{eff}}$  changes with  $\sqrt{s}$ , then the inclusive double 2-jet cross section  $\sigma_D$  would differ from the value shown in Fig. 4 by a factor  $14.5 \text{ mb}/\sigma_{\text{eff}}(\sqrt{s})$ . A table with numerical values for double dijet cross sections, entering Figures 4 and 5, is provided in the electronic supplement to this paper.

At the Tevatron Run I ( $\sqrt{s} = 1.8 \text{ TeV}$ ), the inclusive double dijet cross section reaches  $\approx 20 \text{ nb}$  for  $E_{T,\text{min}} \simeq 20 \text{ GeV}$ . Upon increasing the jet energy threshold, this cross section drops rapidly to  $\approx 20 \text{ pb}$  for  $E_{T,\text{min}} \simeq 40 \text{ GeV}$ . The kinematical reach at the LHC ( $\sqrt{s} = 14 \text{ TeV}$ ) is much wider. With a cross section of  $\approx 16 \text{ nb}$ , one gets to  $E_{T,\text{min}} \simeq 50 \text{ GeV}$ , and with a cross section of  $10 \text{ pb}$ , one explores the scale dependence of  $\sigma_D$  up to  $E_{T,\text{min}} \simeq 120 \text{ GeV}$ .

To put these cross sections into perspective, let us assume an integrated luminosity for Run II at Tevatron of  $10 \text{ fb}^{-1}$  (more than  $6 \text{ fb}^{-1}$  have been delivered to date). This would translate into  $2 \times 10^8$  double dijet events with  $E_{T,\text{min}} \simeq 20 \text{ GeV}$  and  $2 \times 10^5$  events with  $E_{T,\text{min}} \simeq 40 \text{ GeV}$ . (For the purpose of these order of magnitude estimates, we have neglected the difference in center of mass energy between Tevatron Run I and Run II.) To relate the double hard cross section  $\sigma_D$  to a measurable quantity, it is necessary to disentangle the 4-jet events originating from two independent hard scattering processes from those that originate from a single hard scattering. There are various experimental handles for doing this. For instance, one can exploit

that in contributions to  $\sigma_D$ , pairs of two jets must be balanced in  $E_T$ , while contributions from other classes of 4-jet events are not and differ in the shape of their distribution. However, our study does not provide a basis for judging the (experiment-specific) size of event samples, needed for a measurement of  $\sigma_D$ . Here, we assume that  $\sim 10^5$  raw events are sufficient to this end, and we thus estimate that experiments at Tevatron Run II can measure  $\sigma_D$  for  $E_{T,\min} \lesssim 40$  GeV.

Under analogous assumptions, experiments at the LHC will access the physics of double dijet production for  $E_{T,\min} \lesssim 120$  GeV with the first  $10 \text{ fb}^{-1}$  of data at  $\sqrt{s} = 14$  TeV.

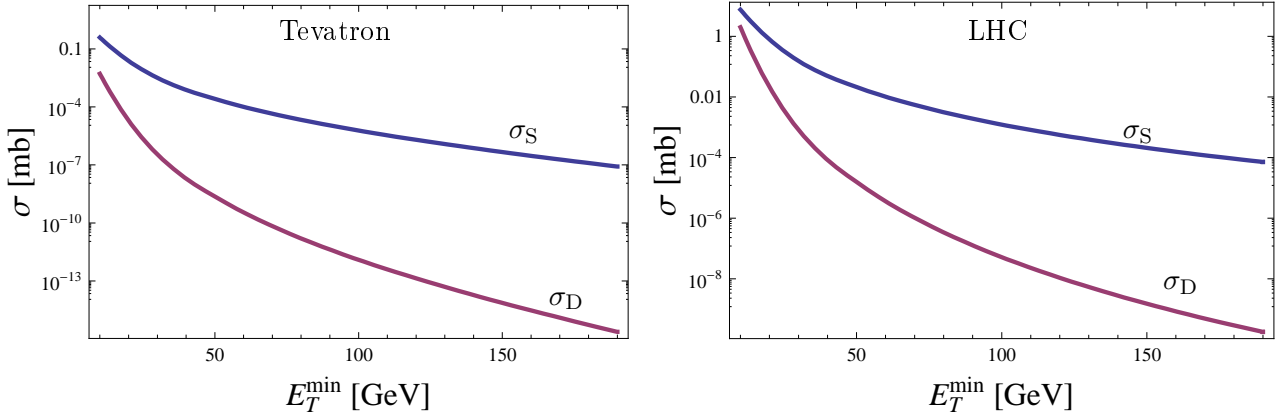


FIG. 4: Calculated inclusive single dijet cross section  $\sigma_S$  (upper curves) and estimated double dijet cross section  $\sigma_D = \sigma_S^2 / (2\sigma_{\text{eff}})$  (lower curves) as a function of the cut on jet transverse energy. Left hand side:  $\sigma_S$  and  $\sigma_D$  at  $\sqrt{s} = 1.8$  TeV. Right hand side:  $\sigma_S$  and  $\sigma_D$  at  $\sqrt{s} = 14$  TeV. The scale factor is assumed to be  $\sigma_{\text{eff}} = 14.5$  mb, independent of  $E_{T,\min}$  and  $\sqrt{s}$ .

### B. The scale dependence of the scale factor $\sigma_{\text{eff}}$

The estimates given in section III A above illustrate that experiments at the LHC can investigate the scale dependence of the scale factor  $\sigma_{\text{eff}}$  over a logarithmically wide range in  $E_{T,\min}$ . We now illustrate the physical information which can be extracted from this scale dependence. To this end, we have calculated the inclusive double dijet cross section (2.4) for two-parton distribution functions (2.5) with Gaussian transverse density profile  $n(x, \mathbf{b})$ . Figure 5 shows results for the corresponding scale factor  $\sigma_{\text{eff}}$ , calculated as a function of  $\sqrt{s}$  and  $E_{T,\min}$  for the

cases of a logarithmic and a power law  $x$ -dependence of the width  $\delta(x)$  of the parton density  $n(x, \mathbf{b})$  in the hadronic projectile.

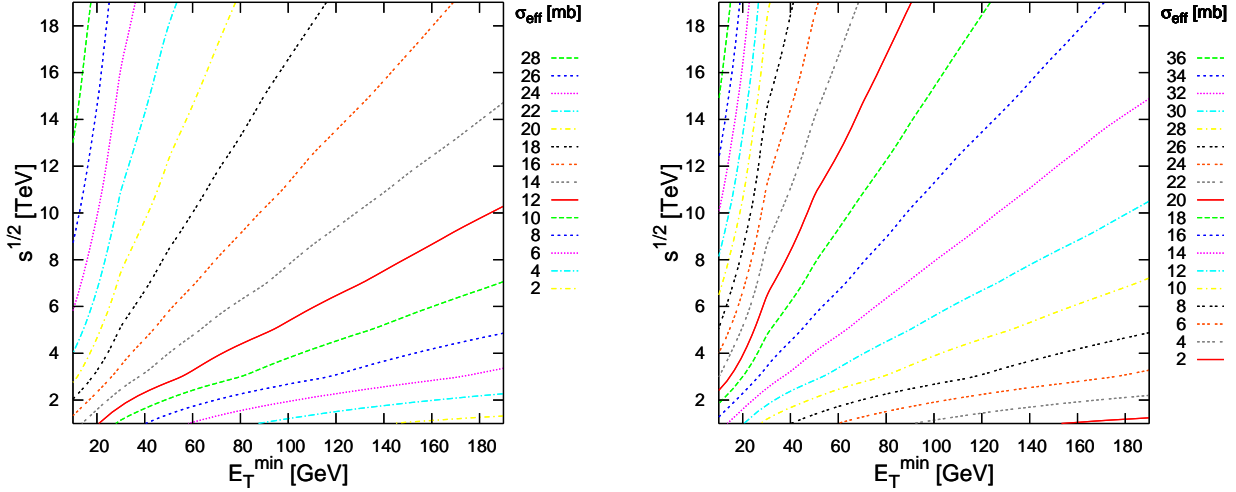


FIG. 5: Theoretical calculation of the scale factor  $\sigma_{\text{eff}} = \sigma_S^2(E_{T,\text{min}}, \sqrt{s}) / 2\sigma_D(E_{T,\text{min}}, \sqrt{s})$  in the plane of center of mass energy  $\sqrt{s}$  and jet energy threshold  $E_{T,\text{min}}$ . Constant  $\sigma_{\text{eff}}$ -values indicated on the right of the two plots lie on approximately straight lines. Inclusive single and double dijet cross sections are calculated from (2.1) and (2.4) respectively, for a Gaussian transverse density distribution of partons in the proton wave function. The  $x$ -dependence of the width of these density distributions is taken to follow a logarithmic increase (2.14) [plot on left hand side] or a power-law increase (2.15) [plot on right hand side]. Model parameters are chosen such that  $\sigma_{\text{eff}} = 14.5$  mb for  $\sqrt{s} = 1.8$  TeV and  $E_{T,\text{min}} = 20$  GeV.

We expect that experimental data on  $\sigma_{\text{eff}}$  at the LHC will first become available as a function of  $E_{T,\text{min}}$  for fixed  $\sqrt{s}$ . However, the foreseen running schedule of LHC may also lead to information about the  $\sqrt{s}$ -dependence of double dijet cross sections. This is so, since before moving to  $\sqrt{s} = 14$  TeV, LHC is scheduled to start operation this year with  $\sqrt{s} = 10$  TeV, aiming for an integrated luminosity of  $200 \text{ pb}^{-1}$  which may be sufficient to explore double hard collisions over a range in  $E_{T,\text{min}}$ . Moreover, at a later stage in the LHC program, one may also expect a relatively short proton-proton run at  $\sqrt{s} = 5.5$  TeV to collect comparison data for the LHC heavy ion program. In addition, data from Tevatron Run II may provide information

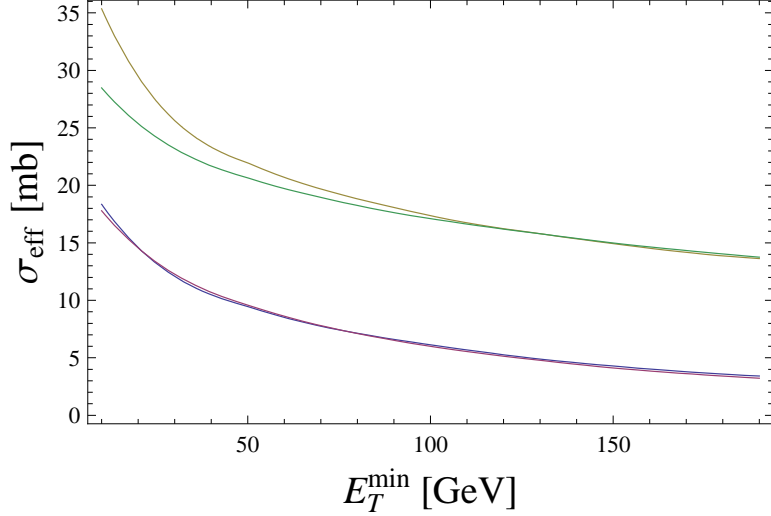


FIG. 6: The scale factor  $\sigma_{\text{eff}}$  for the two models of an  $x$ -dependent width of the Gaussian density distribution, shown in Fig. 3. Upper curves for  $\sqrt{s} = 14$  TeV, lower curves for  $\sqrt{s} = 1.8$  TeV.

about the  $E_{T,\text{min}}$  dependence of  $\sigma_D$  at  $\sqrt{s} = 1.96$  TeV. Measurements of the  $\sqrt{s}$ -dependence of  $\sigma_D(E_{T,\text{min}})$  will test the constancy of  $\sigma_{\text{eff}}$  along lines of constant  $E_{T,\text{min}}/\sqrt{s}$ . This constancy does not depend on details of the modeling of two-parton distribution functions, but results solely from the kinematic bound (2.2). This makes it an important consistency check for the picture of double dijet production advocated here. The main dynamical information of the measurement of  $\sigma_{\text{eff}}$  is contained in its dependence on  $E_{T,\text{min}}$  and  $\sqrt{s}$ . The variation of this scale factor with kinematical variables reflects the growth of the transverse size of the projectile wave function with  $\ln 1/x$ . Fig. 5 illustrates this point for the two models of the transverse growth represented in Fig. 3. One sees that the scale factor increases significantly with increasing  $\sqrt{s}$  or decreasing  $E_{T,\text{min}}$ . We emphasize that at  $\sqrt{s} = 14$  TeV, results of both models shown in Fig. 5 imply a variation of  $\sigma_{\text{eff}}$  by roughly a factor 2 in the range between  $E_{T,\text{min}} = 10$  GeV and  $E_{T,\text{min}} = 100$  GeV. This variation is much larger than the  $\sim 20\%$  measurement uncertainty quoted by the CDF Collaboration for its measurement of  $\sigma_{\text{eff}}$ . We take this as a strong indication that the  $x$ -evolution of the transverse size of hadronic wave functions in the range of semi-hard  $x$  is experimentally accessible via the measurement of double hard cross sections at the LHC.

Once a non-trivial  $E_{T,\text{min}}$ -dependence of the scale factor  $\sigma_{\text{eff}}$  is established, one may ask the refined question of whether this allows for the discrimination between different models of small- $x$  evolution. Since parton distributions  $f(x, Q^2)$  rise rapidly with increasing  $\ln 1/x$ , the inclusive single and double dijet cross sections  $\sigma_S(E_{T,\text{min}})$ ,  $\sigma_D(E_{T,\text{min}})$  are dominated by  $x$ -values which

lie close to the lower bound of (2.2). As a consequence, the value of  $\sigma_{\text{eff}}$  remains almost constant along lines of constant  $E_{\text{T,min}}/\sqrt{s}$  in the  $(E_{\text{T,min}}, \sqrt{s})$  plane. As an estimate, one may take

$$\sigma_{\text{eff}} \simeq 15 \delta^2(x_{\text{min}}^{1/2}), \quad (3.1)$$

where  $x_{\text{min}}$  is the lower bound on the parton momentum fraction available for a dijet above  $E_{\text{T,min}}$  (see Eq. 2.2). Figure 6 shows in more detail that for the two models of  $x$ -evolution shown in Fig. 3, the steeper  $x$ -dependence in the transverse density profile  $n(x, \mathbf{b})$  is indeed reflected in a steeper  $E_{\text{T,min}}$ -dependence of  $\sigma_{\text{eff}}$ . The model-dependent difference is more pronounced for the higher LHC center of mass energy and for lower values of  $E_{\text{T,min}}$ , where double hard scattering processes depend on parton distributions at smaller momentum fraction  $x$ . However, the differences are rather mild and may be difficult to disentangle experimentally. Moreover, the interpretation of relatively small variations in  $\sigma_{\text{eff}}$  may require a more detailed understanding of the geometrical distributions entering  $F_D$  (see section IV below). Thus, while a non-trivial  $E_{\text{T,min}}$ -dependence of  $\sigma_{\text{eff}}$  will allow one to disentangle models of small- $x$  growth from the baseline of an  $x$ -independent transverse localization of partons in the proton, the discrimination between different models of small- $x$  growth may be more challenging.

#### IV. CORRELATED TWO-PARTON DISTRIBUTIONS

So far, we have discussed factorized two-parton distributions of the form (2.5). This ansatz is based on a picture, in which partons are centered around a single position  $\mathbf{b}_v \equiv 0$  in transverse space. The purpose of this section is to gain some understanding of the extent to which the results reached above depend on the geometrical assumptions underlying the ansatz (2.5), and to what extent they reflect dynamical information. To this end, we shall study a simple model of two-parton distributions, which do not factorize into single-parton distributions. The model is based on picturing the transverse profile of the proton projectiles as being composed of three regions of size  $\sim 0.2 - 0.4$  fm each, which have increased hadronic interaction probability. The centers  $\mathbf{b}_{v_i}, i = 1, 2, 3$ , of these hot spots may be thought to be related to the positions of valence quarks in the transverse plane. To be specific, we consider for these hot spots the distribution [25]

$$|\psi(\mathbf{b}_{v_1}, \mathbf{b}_{v_2})|^2 = \frac{3}{\pi^2 \delta_v^4} \exp \left[ -\frac{1}{3\delta_v^2} ((\mathbf{b}_{v_1} - \mathbf{b}_{v_2})^2 + (\mathbf{b}_{v_1} - \mathbf{b}_{v_3})^2 + (\mathbf{b}_{v_2} - \mathbf{b}_{v_3})^2) \right] \Big|_{-\mathbf{b}_{v_3} \equiv \mathbf{b}_{v_1} + \mathbf{b}_{v_2}} \quad (4.1)$$

Here due to the center of mass constraint the third coordinate is defined as  $\mathbf{b}_{v_3} \equiv -\mathbf{b}_{v_1} - \mathbf{b}_{v_2}$ . We fix  $\delta_v = 0.25$  fm, which corresponds to a separation of the centers of the three hot spots by an rms of 0.3 fm. Partons are located around the centers  $\mathbf{b}_{v_i}$  of these hot spots at transverse positions  $\mathbf{b}$  with Gaussian distributions

$$d(x, \mathbf{b}, \mathbf{b}_v) = \frac{1}{2\pi\delta_s(x)^2} \exp\left(-\frac{(\mathbf{b}_v - \mathbf{b})^2}{2\delta_s(x)^2}\right). \quad (4.2)$$

We allow for an  $x$ -dependence of the Gaussian width  $\delta_s$ . A two-parton density distribution  $n_D(x_1, x_2, \mathbf{b}_1, \mathbf{b}_2)$  for partons located at transverse positions  $\mathbf{b}_1, \mathbf{b}_2$  can then be calculated in terms of the following integral over the centers of the hot spots  $\mathbf{b}_{v_i}$ ,

$$n_D(x_1, x_2; \mathbf{b}_1, \mathbf{b}_2) = \frac{1}{4} \int d\mathbf{b}_{v_1} d\mathbf{b}_{v_2} |\psi(\mathbf{b}_{v_1}, \mathbf{b}_{v_2})|^2 \sum_{ij}^2 d(x_1, \mathbf{b}_1, \mathbf{b}_{v_i}) d(x_2, \mathbf{b}_2, \mathbf{b}_{v_j}). \quad (4.3)$$

Here, the sum over  $i$  and  $j$  averages over the different combinations of hot spots in one proton which can provide the two partons for the hard scattering process. In this class of models, the two-parton distribution functions do not factorize, but take the form

$$F_D^{ik}(x_1, x_2; \mathbf{b}_1, \mathbf{b}_2; Q_1^2, Q_2^2) = n_D(x_1, x_2; \mathbf{b}_1, \mathbf{b}_2) f^i(x_1, Q_1^2) f^k(x_2, Q_2^2). \quad (4.4)$$

The corresponding integration over transverse directions, entering (2.3) reads

$$\begin{aligned} & \int d\mathbf{b} ds_1 ds_2 n_D(x_1, x_2; \mathbf{b} - \mathbf{s}_1, \mathbf{b} - \mathbf{s}_2) n_D(x_3, x_4; \mathbf{s}_1, \mathbf{s}_2) \\ &= \frac{1}{8\pi} \left( \frac{1}{\delta_\Sigma^2} + \frac{1}{\delta_\Sigma^2 + 2\delta_v^2} + \frac{2}{\delta_\Sigma^2 + \delta_v^2} \right), \end{aligned} \quad (4.5)$$

where

$$\delta_\Sigma^2 = \delta_s(x_1)^2 + \delta_s(x_2)^2 + \delta_s(x_3)^2 + \delta_s(x_4)^2. \quad (4.6)$$

In the limit  $\delta_v \rightarrow 0$ , one recovers the model of a density distribution with Gaussian profile, discussed in section III. More precisely, for  $\delta_v \rightarrow 0$ , the centers of the three hot spots are all located at  $\mathbf{b}_{v_1} = \mathbf{b}_{v_2} = \mathbf{b}_{v_3} = 0$ , as can be seen from (4.1). For the case of an  $x$ -independent density  $\delta_s(x) = \delta_s$ , Eq. (4.5) becomes  $\frac{1}{8\pi} \frac{4}{\delta_s^2} = \frac{3}{8\pi \langle \mathbf{r}^2 \rangle}$  with  $\langle \mathbf{r}^2 \rangle = 3\delta_s^2$ . This is exactly the value of  $\int d\mathbf{b} T_{NN}^2(\mathbf{b}) = 1/\sigma_{\text{eff}}$  for the Gaussian profile, obtained in Tab. I.

To study the effect of non-factorizing distributions and compare to the results of section III we make use of the Gaussian width  $\delta_{\text{eff}}^2 = \delta_s(x)^2 + \delta_v^2/3$  of the corresponding one-particle distribution  $n(x_1, b_1) = \int d\mathbf{b}_2 n_D(x_1, x_2; \mathbf{b}_1, \mathbf{b}_2)$ . We connect the correlated one-particle distribution

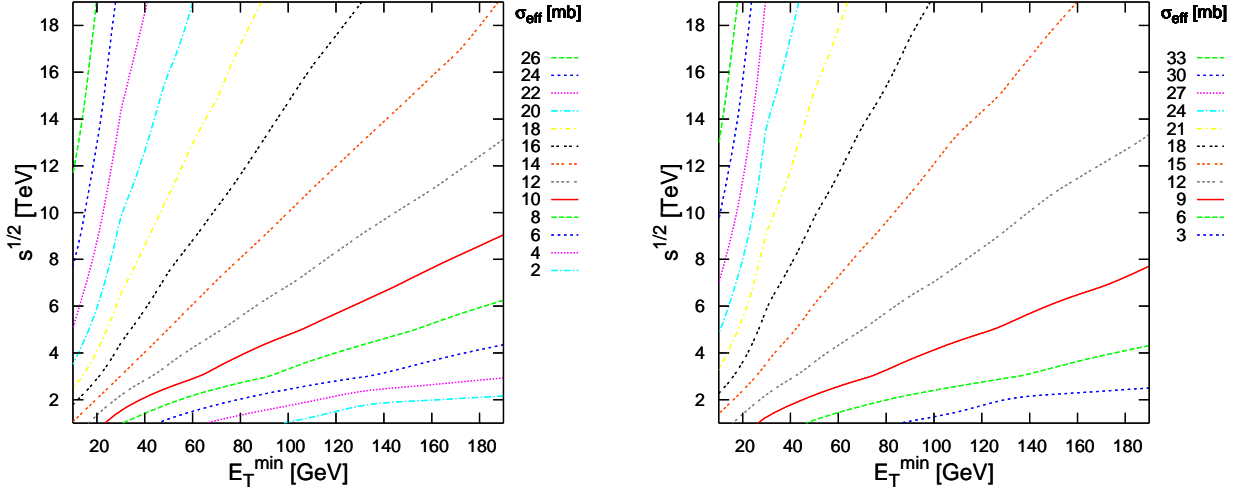


FIG. 7: Same as Fig. 5, but for a model of two-parton distribution functions, for which partons are localized in three hot spots in the parton wave function.

of soft partons to the uncorrelated one by demanding that they have the same Gaussian width,  $\delta(x) = \delta_{\text{eff}}$ . This yields  $\delta_s$  used for the numerical computation.

We have calculated the inclusive double dijet cross section (2.5) for the correlated two-parton distribution function (4.4) and compare again a power-law  $x$ -dependence of the form (2.15) with a logarithmic  $x$ -dependence of the form (2.14). The results of this calculation are shown in Figure 7.

Similar to the calculation with factorized two-parton distribution functions (2.5) shown in Fig. 5, we observe from Fig. 7 that the scale factor  $\sigma_{\text{eff}}$  increases with increasing  $\sqrt{s}$  or decreasing  $E_{T,\text{min}}$ . The numerical differences between the results shown in Fig. 7 and Fig. 5 are relatively small. This may be understood by observing that the average distance between the centers of the hadronically active regions is  $\sqrt{\langle(\mathbf{b}_{v_1} - \mathbf{b}_{v_2})^2\rangle} = \sqrt{2} \delta_v \approx 0.35 \text{ fm}$  for  $\delta_v = 0.25 \text{ fm}$ . The average distance from the center  $\mathbf{b}_{v_i}$ , at which partons are localized is  $\sqrt{\langle\mathbf{b}^2\rangle} = \sqrt{2(\delta_v^2/3 + \delta_s^2(x))} \geq \sqrt{2/3}\delta_v$ . This is  $\approx 0.20 \text{ fm}$  at large  $x$  and increases significantly for smaller  $x$ . As a consequence, the three hadronically active regions in the model (4.3) overlap significantly for our choice of model parameters, and measurable properties of this distribution are likely to be similar to those of the single homogeneous density distribution, studied in section III.

## V. DISCUSSION

In this paper, we have argued that the proton wave function is expected to grow in the transverse plane with increasing  $\ln 1/x$  for all values of  $x$ . We have then illustrated in model studies that this transverse growth should manifest itself in two-parton distribution functions and that it becomes experimentally accessible in the inclusive double dijet cross section  $\sigma_D$ . Of particular interest is the ratio  $\sigma_{\text{eff}} = \sigma_S^2/2\sigma_D$  of the square of the inclusive single over the double dijet cross section. As a generic consequence of the picture advocated here, the scale factor  $\sigma_{\text{eff}}$  is expected to be constant along lines of constant  $E_{T,\text{min}}/\sqrt{s}$ , and it is expected to grow with  $\sqrt{s}$  at fixed jet energy threshold  $E_{T,\text{min}}$  and to decrease with increasing  $E_{T,\text{min}}$  at fixed  $\sqrt{s}$ . We have shown that the wider kinematical reach of proton-proton collisions at the LHC will allow for the first time to test this scale dependence of the scale factor  $\sigma_{\text{eff}}$  over a wide range in  $E_{T,\text{min}}$ .

We have studied models for parton distributions in the transverse plane, which do not distinguish between gluons and valence and sea quarks of different flavor. In the absence of experimental information about such differences, we have adopted the baseline assumption that the geometrical distributions of all partons are the same, thus minimizing the number of model parameters. We note, however, that one may invoke QCD-inspired pictures for which different parton species are localized differently in the transverse wave function. In this case, the scale factor  $\sigma_{\text{eff}}$  can depend on the production channel of the double hard scattering process, since different production channels (such as final states with two-jet events or with  $b\bar{b}$ ) depend on different parton densities. A model, which shows this feature, was studied for instance by Del Fabbro and Treleani in Ref. [23]. The study of specific double hard production channels has also been explored as a means to arrive at an improved (ideally: background free) experimental characterization of double parton collisions. In particular, the production of two equal sign W bosons at relatively low transverse momentum is dominated by double parton collisions [26], though the cross section is very low. A much more abundant channel at the LHC, even if  $b$ -tagging efficiency is taken into account, is the production of  $b\bar{b}b\bar{b}$ , which may allow for an improved characterization of double hard cross sections [28].

The models explored in the present paper result in an increase of  $\sigma_{\text{eff}}$  with increasing  $\sqrt{s}$ . In contrast, the spatial correlations, implemented in the model of Ref. [23], imply that scale factors for all production channels decrease with increasing  $\sqrt{s}$ . This illustrates that the models

studied in the present work do not exhaust all conceivable scale dependencies of  $\sigma_{\text{eff}}$ . The models in section III and IV are simple implementations of the picture that the transverse proton wave function grows with  $\ln 1/x$ . Moreover, the difference between our models and the models of Ref. [23] illustrates clearly, that far beyond producing only an experimental value for  $\sigma_{\text{eff}}$ , a measurement of inclusive double hard cross sections at the LHC can distinguish between qualitatively different pictures of the transverse proton wave function. As we have argued here, this may be done most efficiently by studying the  $E_{T,\text{min}}$ -dependence of the scale factor  $\sigma_{\text{eff}}$  at fixed  $\sqrt{s}$ .

### Acknowledgments

We thank Tom LeCompte, Tilman Plehn, Steffen Schumann and Daniele Treleani for useful discussions. S.D. has been supported within the framework of the Excellence Initiative by the German Research Foundation (DFG) through the Heidelberg Graduate School of Fundamental Physics (grant number GSC 129/1).

- 
- [1] C. Goebel, F. Halzen and D. M. Scott, *Phys. Rev. D* **22** (1980) 2789.
  - [2] N. Paver and D. Treleani, *Nuovo Cim. A* **70** (1982) 215.
  - [3] F. Halzen, P. Hoyer and W. J. Stirling, *Phys. Lett. B* **188** (1987) 375.
  - [4] M. L. Mangano, *Z. Phys. C* **42** (1989) 331.
  - [5] R. M. Godbole, S. Gupta and J. Lindfors, *Z. Phys. C* **47** (1990) 69.
  - [6] F. Abe *et al.* [CDF Collaboration], *Phys. Rev. D* **47** (1993) 4857.
  - [7] F. Abe *et al.* [CDF Collaboration], *Phys. Rev. Lett.* **79** (1997) 584. and *Phys. Rev. D* **56** (1997) 3811.
  - [8] A. Del Fabbro and D. Treleani, *Phys. Rev. D* **61** (2000) 077502 [arXiv:hep-ph/9911358].
  - [9] T. Sjostrand and M. van Zijl, *Phys. Rev. D* **36** (1987) 2019.
  - [10] T. Sjostrand and P. Z. Skands, *JHEP* **0403** (2004) 053 [arXiv:hep-ph/0402078].
  - [11] M. Bahr, S. Gieseke and M. H. Seymour, *JHEP* **0807** (2008) 076 [arXiv:0803.3633 [hep-ph]].
  - [12] M. Drees and T. Han, *Phys. Rev. Lett.* **77** (1996) 4142 [arXiv:hep-ph/9605430].
  - [13] G. Calucci and D. Treleani, *Phys. Rev. D* **60**, 054023 (1999) [arXiv:hep-ph/9902479].

- [14] L. V. Gribov, E. M. Levin and M. G. Ryskin, Phys. Rept. **100** (1983) 1.
- [15] G. P. Salam, Nucl. Phys. B **461** (1996) 512 [arXiv:hep-ph/9509353].
- [16] A. Kovner and U. A. Wiedemann, Phys. Rev. D **66** (2002) 034031 [arXiv:hep-ph/0204277].
- [17] H. Weigert, Prog. Part. Nucl. Phys. **55** (2005) 461 [arXiv:hep-ph/0501087].
- [18] A. I. Shoshi, F. D. Steffen and H. J. Pirner, Nucl. Phys. A **709** (2002) 131 [arXiv:hep-ph/0202012].
- [19] J. Pumplin, D. R. Stump, J. Huston, H. L. Lai, P. M. Nadolsky and W. K. Tung, JHEP **0207** (2002) 012 [arXiv:hep-ph/0201195].
- [20] T. Sjostrand, S. Mrenna and P. Skands, JHEP **0605** (2006) 026 [arXiv:hep-ph/0603175].
- [21] H. J. Pirner, B. Galow and O. Schlaudt, Nucl. Phys. A **819** (2009) 135.
- [22] M. Burkardt, Int. J. Mod. Phys. A **18**, 173 (2003) [arXiv:hep-ph/0207047].
- [23] A. Del Fabbro and D. Treleani, Phys. Rev. D **63**, 057901 (2001) [arXiv:hep-ph/0005273].
- [24] M. Strikman and C. Weiss, arXiv:hep-ph/0408345.
- [25] I. Bender, H. G. Dosch, H. J. Pirner and H. G. Kruse, Nucl. Phys. A **414** (1984) 359.
- [26] A. Kulesza and W. J. Stirling, Phys. Lett. B **475** (2000) 168 [arXiv:hep-ph/9912232].
- [27] B. Z. Kopeliovich, I. K. Potashnikova, B. Povh and I. Schmidt, Phys. Rev. D **76** (2007) 094020 [arXiv:0708.3636 [hep-ph]].
- [28] T. LeCompte, private communication.